CHAPTER

13

A review of transport of nanoparticles in porous media: from pore- to macroscale using computational methods

Gianluca Boccardo[1], Tiziana Tosco[2], Asako Fujisaki[3], Francesca Messina[4], Amir Raoof[3,5], David R. Aguilera[6,3], Eleonora Crevacore[7], Daniele L. Marchisio[1], Rajandrea Sethi[2]

[1]DISAT – Dipartimento di Scienza Applicata e Tecnologia – Politecnico di Torino, Torino, Italy; [2]DIATI – Dipartimento di Ingegneria dell'Ambiente, del Territorio e delle Infrastrutture – Politecnico di Torino, Torino, Italy; [3]DELTARES, Department Subsurface and Groundwater Quality, Utrecht, The Netherlands; [4]The Water Institute of the Gulf, Baton Rouge, LA, United States; [5]Environmental Hydrogeology Group, Department of Earth Science, Utrecht University, Utrecht, Netherlands; [6]DELTARES, Department User Interface Software, Delft, The Netherlands; [7]DISMA - Dipartimento di Scienze Matematiche – Politecnico di Torino, Torino, Italy

Chapter outline

Nanomaterials for the Detection and Removal of Wastewater Pollutants. https://doi.org/10.1016/B978-0-12-818489-9.00013-X

1. Introduction

Transport and deposition of colloidal particles in saturated porous media is of great importance in many fields of science and engineering. On the one hand, mobile subsurface colloids have received considerable attention due to their potential risk for human health since natural colloids can act as a carrier for a wide range of harmful contaminants by strong absorption, thus extremely facilitating their migration in the subsurface. On the other hand, study of colloids is related to the development of new remediation technologies. Prediction of transport and fate of colloidal particles in the subsurface environment requires a thorough understanding of particle filtration processes. Mechanisms that control the mobility of reactive nano- (and micro-) particles determine the design, implementation, and performance evaluation of remediation field applications [80].

For engineering applications, particle transport and deposition are the basis of deep-bed granular filtration, commonly adopted in water and wastewater treatment and industrial separation processes [81]. Particle removal efficiency and head loss across the packed bed depend on a number of parameters, including suspension properties (e.g., particle size distribution and concentration, particle surface chemistry, and solution chemistry), filter design parameters (e.g., media size, type, and depth), and operating conditions (e.g., filtration rate and filter runtime) [18]. Even though empirical or semiempirical approaches are available for the design of filters in many industrial applications, several aspects related to colloid retention mechanisms are still not fully understood.

Another application of colloid filtration processes is in the field of petroleum engineering, where fine migration and clogging in the vicinity of the production wells may be a critical issue for well efficiency and oil or gas production [92].

Colloid transport is a peculiar multiscale problem where pore-scale phenomena have an important impact on the transport at larger scales. Particles migrating through a porous medium may remain in the solution phase and be transported due to the advection and dispersion processes or be retained due to the filtration (when particle size exceeds the pore size or particle is entrapped in the dead-end pores) and deposition onto the porous matrix (a phenomenon controlled by physicochemical particle−particle and particle−porous medium interactions). In the past few decades, there has been a very large increase in the use of pore-scale modeling to study (multiphase) flow and (reactive) transport in porous media [6] to gain a better understanding of the mechanisms underlying colloidal deposition and aggregation by studying the intergranular dynamics [22].

The complex and random arrangement of soil grains, which determines the hydrodynamics of the system, is very difficult, if not impossible, to be described in detail in a mathematical framework at this time. This problem, related to the complexity of the system, can be approached in two different ways [18]:

- The physical system can be approximated crudely enough assuming that an exact mathematical solution to the problem is obtainable (analytical solution).
- A more accurate representation of the system can be used, which would require an approximate, numerical, solution.

For larger domain sizes (e.g., laboratory-scale colloid transport), the solution of flow and transport equations within each individual pore is not feasible, and up-scaled continuum averaged equations are to be utilized. However, for solving large-scale problems (e.g., multidimensional representation of field-scale processes), continuum-scale modeling approaches are still under development, and up-scaled kinetics, based on the underlying pore-scale processes, are still missing.

Two major theoretical methods are available to simulate colloid transport and to calculate the particle deposition rate onto the porous medium, namely, Lagrangian and Eulerian approaches. Lagrangian methods describe the trajectory of the particle as it comes near the collector surface, whereas Eulerian ones describe the evolution of particle concentration in time and space [21]. The Lagrangian approach is therefore suitable for the representation of the trajectory of individual particles at a microscopic level [22]. Conversely, the Eulerian method describes the particles collectively, in terms of their distribution or probability density function, in time and space, and is consequently a typical macroscopic approach [22,81,91].

Even though the Lagrangian approach is, in principle, capable of dealing with Brownian particles, it has been typically used to describe non-Brownian particles motion because their trajectories are deterministic and easier to express analytically. The representation of Brownian motion requires addition of a thermal random force in the equation of motion, leading to a Langevin's form equation, the solution of which results in stochastic trajectories [11,21]. The solution of such equations requires laborious and time-consuming integration of the stochastic equation of motion [22] and is in practice only feasible for a limited number of particles from a practical point of view.

Eulerian methods have been the most widely employed approach for describing transport and deposition phenomena at larger scales. Using Eulerian methods, the difficulty of accounting for Brownian effects is eliminated, and these methods are more amenable to numerical or approximate analytical solutions [21]. For this reason, the Lagrangian approach was less attractive than the Eulerian approach, especially before the widespread availability of high-performance computers.

This review on pore-scale modeling covers five main topics: (1) techniques to mimic the soil structure, (2) hydrodynamics of the porous medium, (3) particle transport mechanics, (4) particle–particle and particle–porous medium interactions, and (5) up-scaling from pore scale to macroscale. We begin by introducing the methods to represent the pore structure, at different levels of simplifications. Fluid flow solutions are then discussed, focusing in particular on laminar and Newtonian flow, which is the condition encountered in the majority of applications of particle transport problems (especially for subsurface water flow). Finally, different approaches developed to represent and quantify particle transport and deposition in porous media are presented and discussed, highlighting possible critical points and aspects, which need to be further elucidated. Finally, we briefly discuss up-scaling approaches based on pore-scale processes, appropriate to be used in macroscale modeling.

2. Pore-scale modeling

2.1 Pore space representation

At the pore scale, the solid phase of the porous medium is represented as an assembly of grains (i.e., collectors), whose structure, geometry, and size distribution must be known in detail [78]. The geometry of the collectors can be simplified (e.g., as spheres), or realistic, directly obtained from imaging of a real sample (for example, a packed sand sample). Single grain or multiple packed grains (multiple collectors) can be considered in both two and three dimensions. An overview of the commonly adopted geometric representations is given in Fig. 13.1. The simplest representation of a single collector is a sphere, which is typically studied as a circle in 2D, by exploiting the radial symmetry of the collector. To explore the influences of grain shape (sphericity) and surface roughness, nonspherical collectors have been also considered [12,73]. Several configurations have been proposed

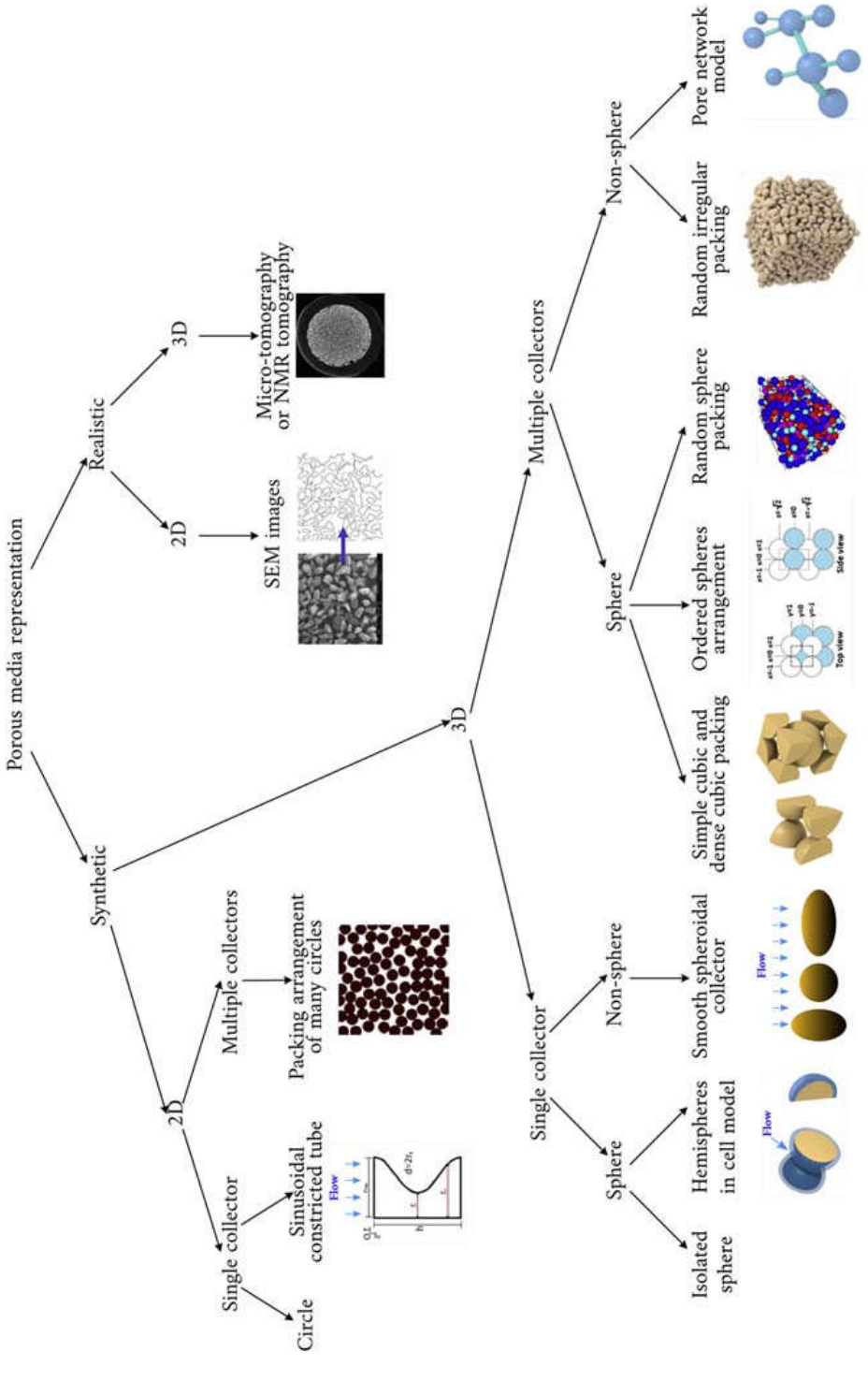

FIGURE 13.1

Various geometric representations of porous media.

to take into account the impact of grain-to-grain contacts and pore space configuration on particle transport and retention, namely, the hemispheres-in-cell model, which incorporates grain-to-grain contact [49]; the simple cubic packing and dense cubic packing [16,17,36]; the sinusoidal constricted tube accounting for the geometry nature of the pores; and the impact of constricted passages [88].

At a larger scale, when several packed collectors are considered, synthetic 2D or 3D geometries usually adopt an assembly of irregular (realistic) grains [8] or circles (or spheres) arranged in a regular pattern [18] or randomly packed [15,35,67]. Another approach is pore network modeling, in which several pores are connected using capillary channels to represent the void space. In the simplest case, pores are located at a regular lattice, whereas in more complex pore network models, a large variety of irregular networks can be selected [5,24,47].

2.1.1 Realistic pore-scale geometries

Realistic representations of the pore space geometry in both 2D and 3D are less common at the moment, compared with regular structures of packed spheres, since they require significantly higher computational costs, and the reconstruction of the pore space requires specific algorithms. The geometric characteristics of pores and their position can be chosen randomly from prescribed distributions or alternatively selected to match experimentally determined pore space geometries [9,52].

In some recent works employing this methodology, a code performing rigid body dynamics [9,63] or discrete element method simulations [75] is used to generate a realistic packing by reproducing the gravitational settling of a sufficient number of arbitrarily shaped solid grains; the interaction parameters (e.g., elastic restitution coefficient, friction factor) are specified to obtain experimental values of porosity for the considered packing.

Then, having obtained this in silico porous media model, this geometrical representation is then passed to a computational fluid dynamics (CFD) code solving the appropriate physical equations to be studied.

Alternatively, the structure of a granular media can be obtained by carrying out image analyses of real samples. For 2D domains, SEM images of grains can be used [80], and 3D digital images can be obtained from high-resolution three-dimensional X-ray tomography or NMR tomography experiments [1,61].

2.1.2 Pore-network models

Traditionally, approaches based on pore-network models have been one of the most common pore-scale modeling methods. Pore-network models require extensive preprocessing (network extraction) to discretize the imaged irregular pore space into simple pore elements (mostly represented as pore bodies and pore throats). To mimic realistic porous media processes, network models should reproduce the main morphological and topological features of real porous media (Fig. 13.2). These should include pore-size distribution and pore coordination number and connectivity. The coordination number, defined as the total number of pore throats (capillary channels) that connect a given pore to its adjacent ones, has a wide range of variation number in natural porous media. To generate pore spaces with defined pore connectivities, Raoof and Hassanizadeh [70] have developed a multidirectional pore-network approach for representing a porous medium, which allows for a wide range of coordination numbers.

Each representation of the pore space corresponds to a different degree of simplification and, consequently, requires different assumptions when solving flow and transport equations. In the following section, an overview of the major approaches is provided and discussed.

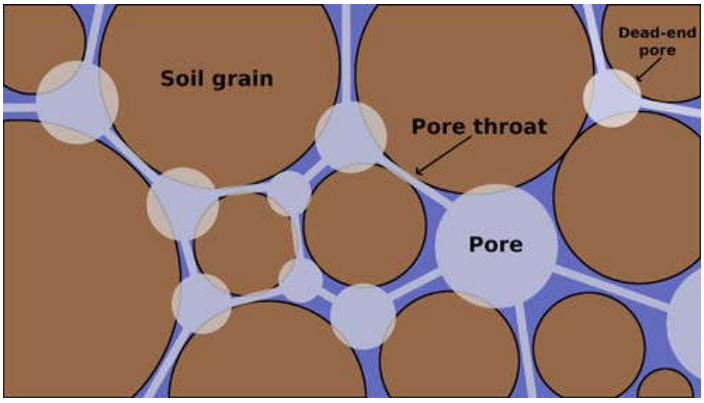

FIGURE 13.2

Pore spaces within a soil matrix, and discretization into spheres (i.e., pore bodies) and capillary tubes (i.e., pore throats), representing the continuum space that the groundwater moves through at the small scale.

2.2 Flow field description

Studying colloid transport, it is commonly assumed that flow and colloid transport are not coupled processes (i.e., the presence of colloidal particles does not affect the flow field, due to the usually low Stokes number). As a consequence, a quantitative description of the undisturbed flow field is an essential prerequisite to the solution of the transport problem [22].

As a general rule, the flow behavior of the carrier fluid is described by mass and momentum conservation equations, usually written in the differential form [25]. The equations can be closed and simplified using approximations and assumptions on the nature of the fluid considered. The most common assumption consists in incompressible and Newtonian fluid [22,25]. In this case, the continuity equation and the Navier–Stokes equations are [22]:

$$\nabla \cdot \boldsymbol{v} = 0 \tag{13.1}$$

$$\frac{\partial \boldsymbol{v}}{\partial t} + \boldsymbol{v} \cdot \nabla \boldsymbol{v} = -\frac{\nabla p}{\rho} + \frac{\mu}{\rho}\nabla^2 \boldsymbol{v} + \boldsymbol{f_e} \tag{13.2}$$

where μ is the constant (dynamic) viscosity, $\boldsymbol{v}$ is the fluid velocity (vector), P is the hydrostatic pressure, and $\boldsymbol{f_e}$ represents the external forces exerted on a unit mass of the fluid. In most cases, a steady state is assumed, and the external forces are neglected, thus leading to the following dimensionless formulation of Eq. (13.2):

$$N_{Re}\widetilde{\boldsymbol{v}} \cdot \nabla \widetilde{\boldsymbol{v}} = -\nabla \widetilde{p} + \nabla^2 \widetilde{\boldsymbol{v}} \tag{13.3}$$

where

$$\widetilde{\boldsymbol{v}} = \frac{\boldsymbol{v}}{U_0}, \quad \widetilde{p} = \frac{pL_0}{\mu U_0}, \quad N_{Re} = \frac{\rho L_0 U_0}{\mu} \tag{13.4}$$

where $\widetilde{\boldsymbol{v}}$ and $\widetilde{p}$ are the normalized (dimensionless) velocity vector and fluid pressure. N_{Re} is the Reynolds number and describes the ratio of inertial forces (linear term $\widetilde{\boldsymbol{v}} \cdot \nabla \widetilde{\boldsymbol{v}}$) to the viscous one

(nonlinear term $\nabla^2\tilde{\boldsymbol{v}}$) [22,25]. The lower the N_{Re} is, the closer the momentum equation is to a linear equation (Stokes equation), and *laminar flow* is retrieved; the higher the N_{Re} is, the more important are the nonlinear terms (Navier–Stokes equation), thus leading to *turbulent flow*. The value of the Reynolds number, and hence the flow regime, is determined by the characteristic length scale and reference velocity. Thus, although a suspension flowing through a pipe at high speed may be turbulent, the local flow field around each suspended particle may still be laminar.

For $N_{Re} << 1$, under steady-state conditions and neglecting external forces, the Stokes or creeping flow equation is obtained:

$$\nabla^2\boldsymbol{v} = \frac{1}{\mu}\nabla p \tag{13.5}$$

which is of importance to analyze flow containing small particles (suspensions) and flow-through porous media and narrow passages [25]. Eq. (13.5) has the advantage of being a linear differential equation, so the superposition technique can be employed to decompose complex flow field into simpler ones [22].

Experience shows that Stokes and Navier–Stokes equations describe the flow of a Newtonian fluid accurately, but, only in few cases and in very simple geometries, it is possible to obtain an exact, analytical solution (e.g., flow around an isolated sphere) [21,78]. In other cases, an analytical solution can be still retrieved, but under simplifying assumptions, acceptable under a restrictive number of hypotheses [25]. However, in general, when simplifying assumptions required for analytical solutions cannot be accepted, or when the pore space geometry is irregular and a detailed flow field is required, a numerical solution can be obtained by performing CFD simulations. In these cases, a key aspect is the selection of the discretization method, i.e., the method of approximating the differential equations by a system of algebraic equations for the variable at some set of discrete locations in space and time. Many approaches are available, whose detailed discussion is beyond the purpose of this study. However, among the approaches more often adopted in the field of colloid transport, finite differences, finite volumes, and finite elements methods are all worth being mentioned. Other methods, such as spectral schemes, boundary element methods, and cellular automata, are employed in CFD, but their use is limited to special problem categories [25].

In the following paragraphs the most commonly used approaches to the solution of the flow field in pore-scale models are summarized. The section is not intended as an exhaustive and complete description of all available models for pore-scale flow simulations, but it focuses specifically on those approaches, which are most used for colloid transport simulations.

2.2.1 Flow past a single sphere

In many cases, a porous medium grain, called collector, may be approximated to a sphere, and the granular medium is represented as a set of collectors, each of them behaving in a similar way. Under such an assumption, spherical coordinates are adopted for a more efficient representation of the domain. In some cases (e.g., isolated sphere, Happel's, and Kuwabara's models), a symmetry along the vertical axis is assumed, and, consequently, the flow is solved in 2D (coordinates r and θ, Fig. 13.3A and B), whereas in other cases a full 3D domain is required (hemisphere-in-cell model, Fig. 13.3C).

The simplest model represents the grain as an *isolated sphere* in an infinite fluid domain, and each grain in the porous medium is totally independent of the others. The flow field around the grain is solved as the flow of fluid of infinite extent over a single sphere, under laminar flow conditions

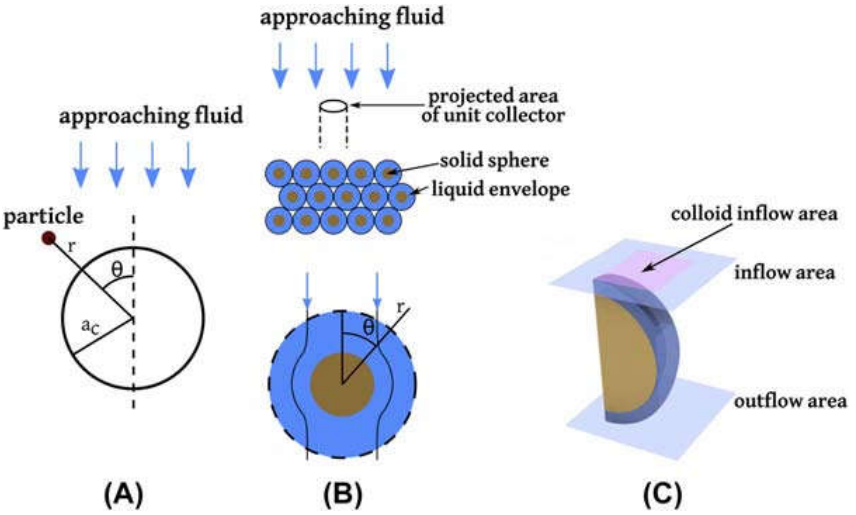

FIGURE 13.3

Schematic description of single sphere models for homogeneous porous media: (A) isolated sphere [21], (B) Happel's model [21], and (C) hemisphere-in-cell model. In (C), the blue planes represents the flow entry and exit surfaces, and the purple region denotes the area in which colloids are randomly introduced [49].

(i.e., Stokes solution). If spherical coordinates with symmetry with respect to the vertical axis are adopted (Fig. 13.3A), then the following boundary conditions can be imposed:

$$v_r = 0, v_\theta = 0, \quad \text{for } r = a_c; \tag{13.6}$$

$$v_r \to -U_\infty \cos\theta, \quad \text{for } r \to \infty; \tag{13.7}$$

$$v_\theta \to -U_\infty \sin\theta \quad \text{for } r \to \infty. \tag{13.8}$$

where r and θ are the coordinates, v_r and v_θ are the components of the fluid velocity along, respectively, r and θ, and U_∞ is the modulus of the undisturbed (vertical) flow velocity.

An analytical solution can be derived for creeping flow ($N_{Re} << 1$) [78]:

$$v_r = -U_\infty \cos\theta\left(\frac{1}{2}\frac{a_c^3}{r^3} - \frac{1}{2}\frac{a_c}{r} + 1\right), \tag{13.9}$$

$$v_\theta = -U_\infty \sin\theta\left(-\frac{1}{4}\frac{a_c^3}{r^3} - \frac{3}{4}\frac{a_c}{r} + 1\right). \tag{13.10}$$

where a_c is the radius of the collector.

A set of single collector models, which also take into account possible modifications to the flow field induced by the other grains, are the so-called sphere-in-cell models, among which Happel's model [30] is the most widely applied one [69,81]. The granular medium is represented as a collection of identical cells consisting of a solid sphere of radius b surrounded by a fluid layer whose thickness b is proportional to porosity n (Fig. 13.3B) as:

$$b = a_c(1-n)^{-\frac{1}{3}} \tag{13.11}$$

The flow field is usually solved by the use of stream functions [69].The equation of motion for the creeping flow [69] is solved assuming symmetry around the vertical axis, and the following boundary conditions are imposed [78]:

$$v_r = 0,\ v_\theta = 0, \quad \text{for } r = a_c, \tag{13.12}$$

$$v_r \to -U_\infty \cos\theta, \quad \text{for } r = b, \tag{13.13}$$

$$\frac{1}{r}\frac{\partial v_r}{\partial \theta} + r\frac{\partial}{\partial r}\left(\frac{v_\theta}{r}\right) = 0, \quad \text{for } r = b, \tag{13.14}$$

Kuwabara's model is identical to Happel's model in conception and formulation but applies different boundary conditions [31,41,78]:

$$v_r = 0,\ v_\theta = 0, \quad \text{for } r = a_c, \tag{13.15}$$

$$v_r \to -U_\infty \cos\theta, \quad \text{for } r = b, \tag{13.16}$$

$$\frac{\partial v_\theta}{\partial r} + \frac{v_\theta}{r} - \frac{1}{r}\frac{\partial v_r}{\partial \theta} = 0 \quad \text{for } r = b, \tag{13.17}$$

The *hemisphere-in-cell model* has been proposed as an extension and generalization of Happel's model to incorporate the effects of a grain-to-grain contact [49]. The spherical collector is represented as a portion (a quarter) of a sphere, surrounded by a shell of fluid. Symmetry planes along the two sections of the sphere and at the portion representing grain-to-grain contacts are applied (Fig. 13.3C). Continuity and steady-state Navier–Stokes equations under laminar flow assumption are solved in spherical coordinates (i.e., r, θ, and φ) by imposing the following boundary conditions [49]:

$$v_r = 0, \quad v_\theta = 0, \quad v_\phi = 0, \quad \text{for } r = a_c, \tag{13.18}$$

$$v_r = U_\infty \cos\theta, \quad \text{for } r = b, \tag{13.19}$$

$$v_\theta = \frac{U_\infty}{2}\sin\theta\left(\frac{-4 + 3\gamma + 5\gamma^3 - 6\gamma^5 + 2\gamma^6}{2 - 3\gamma + 3\gamma^5 - 2\gamma^6}\right), \quad \text{for } r = b, \tag{13.20}$$

$$v_\phi = 0, \quad \text{for } r = b, \tag{13.21}$$

where φ is the third spherical coordinate and $\gamma = (1-n)^{1/3}$ is a function of porosity.

No closed-form solution is available for this model, and the flow field is therefore solved numerically [49].

It is also worth mentioning Brinkman's model [14], another approach that couples the pore-scale accurate solution of the flow field around a sphere with a large-scale, continuum solution of flow at larger distances. In this case, the collector is represented again as a solid sphere of radius a_c, embedded in a granular mass. The flow field far from the collector is solved by applying the Darcy's law, whereas, close to the sphere surface, the Navier–Stokes equation is applied under creeping flow conditions [78]:

$$\nabla p = -\frac{\mu}{k}v + \mu\nabla^2 v \tag{13.22}$$

where $\boldsymbol{k}$ is the permeability tensor.

Imposing the following boundary conditions:

$$v = 0 \quad \text{for } r = a_c, \tag{13.23}$$

$$v = U_\infty \quad \text{for } r \to \infty, \tag{13.24}$$

it is possible to recover the analytical formulation for both the components of the velocity vector, v_r and v_θ.

The above presented models, despite their differences, are all formulated on the assumption that a relatively simple configuration can be used to represent randomly packed granular media, but due to their simplicity, they only approximate realistic porous media [78].

2.2.2 Flow in pore-network models

In pore-network modeling, the relevant conservation laws are solved within each pore element [52]. Pore-network models have been used extensively to simulate multiphase and single-phase fluid flow in porous media, and these models will continue to provide important insight and information in the future. However, pore-network models are based on simplified pore geometries and, in the case of multiphase fluid flow, simplified physics controlling transport of phase interfaces. In addition, pore-network models are less suited for the simulation in fractured media, vuggy carbonates, or other systems with the presence of complex macropores. More recently, a number of methods based more firmly on first principles have been developed. These methods include lattice Boltzmann simulations, particle methods such as dissipative particle dynamics and smoothed particle hydrodynamics, and computational fluid dynamics with fluid−fluid interface tracking/capturing and velocity-dependent contact angles. These methods are computationally less efficient than pore-network models, but the sustained increases in the capability of computing systems are making them more and more attractive [52].

After constructing the skeleton and the geometry of the pore network, it can be applied to model fluid flow and reactive/adsorptive solute transport. Volumetric discharge, q_{ij}, through a given pore throat (such as pore throat ij in Fig. 13.4), can be prescribed by the Hagen−Poiseuille equation [70]:

$$q_{ij} = \frac{\pi R_{ij}^4}{8\mu l}(P_j - P_i) \tag{13.25}$$

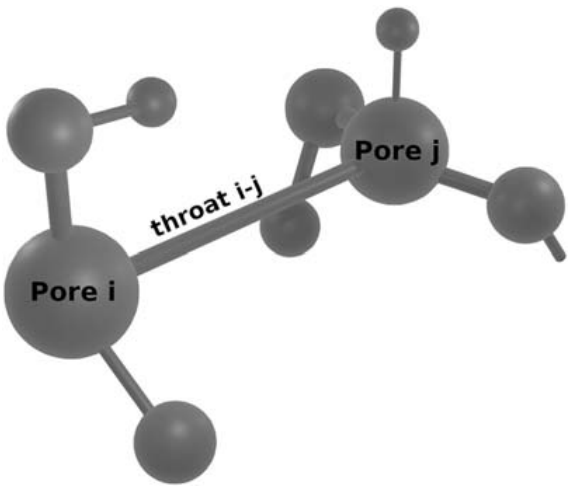

FIGURE 13.4

An example of interconnected pore bodies and pore throats. Flow direction is from pore body *j* into pore body *i* in tube *ij*. Node *j* is the upstream node.

where R_{ij} is the radius of the pore throat, and P_i and P_j are pressures at pore bodies i and j, respectively. For incompressible, steady-state flow, the sum of discharges of pore throats connected to a pore body must be zero:

$$\sum_{j=1}^{z_i} q_{ij} = 0 \quad j = 1, 2, \ldots, z_i \tag{13.26}$$

where z_i is the coordination number of pore body i. Eq. (13.26) is applied to all pore bodies except those on the two flow boundaries where pressures are specified.

The system of Eqs. (13.25) and (13.26) for all pores results in a linear system having a sparse, symmetric, positive-definite coefficient matrix to be solved for pore body pressures. The flow velocity in all pore throats can be calculated using Eq. (13.25).

Considering the network domain as an REV (representative elementary volume), the average pore water velocity, $\overline{v}$, can be determined as:

$$\overline{v} = \frac{QL}{V^f} = \frac{Q}{nS} \tag{13.27}$$

where Q is the total discharge through the network (the sum of fluxes through all pore throats at the inlet or outlet boundary of the network), L is the network length in the flow direction, V^f is the total fluid volume present in the network, n is porosity, and S is the cross-sectional area of the network perpendicular to the overall flow direction.

2.3 Particle transport simulations at the pore scale

Transport of colloids can be studied using two main approaches: the Lagrangian method based on the trajectory analysis of the individual particles [20,64], or the Eulerian method that describes the evolution of particle concentration in time and space [21].

In the Lagrangian approach, the trajectory of a particle around a given collector is determined by the various forces acting on it, which should be described in detail [22]. Flow and transport problems are independent: The flow field around the collector is assumed undisturbed by the presence of the colloidal particles and is obtained by analytical or numerical solutions of the Stokes or Navier−Stokes equation, as described in Section 2.2. The particle trajectory is obtained by solving the classical Langevin's equation, including a balance of all forces acting on the particle:

$$m\frac{d\boldsymbol{u}}{dt} = \boldsymbol{F_{tot}} \tag{13.28}$$

where m is the particle mass, $\boldsymbol{u}$ is the particle velocity vector, and the terms on the right-hand side of the equation are the forces acting on the particle, $\boldsymbol{F_{tot}}$. These forces include fluid drag ($\boldsymbol{F_D}$), gravity ($\boldsymbol{F_G}$), electrostatic ($\boldsymbol{F_{EDL}}$), Van der Waals ($\boldsymbol{F_{VdW}}$), and Brownian forces ($\boldsymbol{F_B}$). Among these forces, $\boldsymbol{F_{EDL}}$ and $\boldsymbol{F_{VdW}}$ only act on the particle in the normal direction relative to the collector surface.

The Eulerian approach is instead based on the solution of the convective diffusive equation:

$$\frac{\partial c}{\partial t} + \nabla\cdot(\mathbf{v}c) = \nabla\cdot(D\nabla c) - \nabla\cdot\left(\frac{\mathbf{D}\cdot\mathbf{F}}{k_B T}c\right) \tag{13.29}$$

where $\boldsymbol{v}$ is local fluid velocity, c is the particle concentration, $\boldsymbol{D}$ is the particle diffusion tensor, k_B is the Boltzmann constant, T is the absolute temperature, and $\boldsymbol{F}$ is the external force vector that takes into account the gravity force and interaction forces (e.g., Van der Waals forces and electric double layer interactions). In this case, the Brownian force is implicitly considered in the diffusion tensor. Quite often, $\boldsymbol{D}$ is considered as a scalar coefficient, normally evaluated with the Stokes–Einstein's formulation:

$$D = \frac{k_B T}{6\pi\mu a_p} \tag{13.30}$$

where T is the absolute temperature and a_p is the particle radius.

2.3.1 Molecular simulation methods

Molecular simulation methods were traditionally employed first to numerically solve microscale problems. Before the considerable improvement in high-performance computational methods, the properties of a molecular substance could be predicted only with theories giving an approximate description of a material. Conversely, when large-scale computational resources were made available, numerical simulation of liquids was one of the first problems to be tackled [27], employing molecular simulation methods.

Such methods operate at a microscopic level dealing with the constituent species of a system, from which macroscopic and microscopic quantities of interest are estimated. The most popular methods are the molecular dynamics (MD) and Monte Carlo (MC) methods. Furthermore, Brownian dynamics (BD), dissipative particle dynamics (DPD), and lattice Boltzmann dynamics (LBD) methods are also widely used, as they are powerful tools to simulate particle dispersion and share some features with the molecular simulations methods.

The classical *molecular dynamics methods* can be employed to simulate a spherical particle dispersion if only the translational motion is considered. However, the method can be applied also to dispersions of nonspherical particles by including also rotational motion [3,2]. In case of spherical particles, for a system of N interacting molecules (or particles), a set of equations expressing Newton's second law can be written, one for each molecule:

$$m\frac{d^2\boldsymbol{r_i}}{dt^2} = \boldsymbol{F_i} \tag{13.31}$$

where i counts the molecules (or particles), t is time, $\boldsymbol{r_i}$ is the position vector, and $\boldsymbol{F_i}$ represents the forces acting on the i-th molecule and takes into account both external fields and the interactions between molecules. The system can be solved transforming Eq. (13.31) into an algebraic equation, approximating every component of the second-order differential term; employing a central difference approximation (second-order accuracy), the *Verlet method* is obtained [83]. If also velocity equations are solved simultaneously, the *velocity Verlet method* is obtained [77], which is significantly superior with respect to the stability and accuracy of simulations.

Since the MD method makes use of the equation of motion, it is applicable to both thermodynamic equilibrium and nonequilibrium phenomena. However, it is quite unfeasible for particle dispersion simulations, since the characteristic times of the motion of the solvent molecules and dispersed particles are considerably different.

In contrast with the MD method, the *Monte Carlo method* does not use the equations of motion but simulates phenomena in thermodynamic equilibrium, where the explicit time is not required. In particular, for N interacting spherical particles, the MC method employs a stochastic law to generate a series of microscopic states, determined by the position vectors $\boldsymbol{r_i}$. The microscopic states are generated according to a probability function, which depends on the position vectors via the interaction energy function $U=U(\boldsymbol{r_1}, \boldsymbol{r_2}, \ldots, \boldsymbol{r_N})$. Among the algorithms available in Monte Carlo methods, the most successfully applied in colloid transport simulations is the *Metropolis* one [32,55], which can deal with both spherical and nonspherical particles.

In the *Brownian dynamics method*, the motion of dispersed particles is taken into account, considering the solvent molecules as a continuum medium, and the solvent influence is included into the equation of motion of dispersed particles as random forces. In particular, when each spherical particle can be regarded as moving independently, the motion is governed by the Langevin equation:

$$m\frac{d\boldsymbol{u}}{dt} = \boldsymbol{F} - \xi\boldsymbol{v} + \boldsymbol{F_B} \tag{13.32}$$

where ξ is the friction factor coefficient $\xi = 6\pi\mu a_p$, $\boldsymbol{F}$ are the external forces, and $\boldsymbol{F_B}$ is the (Brownian) random force. As in molecular dynamics methods, the Brownian motion Eq. (13.32) is solved numerically by transforming it into a system of algebraic equations, approximating position and velocity vectors.

The *dissipative particle dynamics method* is based on a mesoscopic model that allows to simultaneously simulate the motion of fluid and colloid particles: groups or clusters of solvent molecules are seen as virtual particles (dissipative particles), to overcome the differences in characteristic times. This method is particularly useful to take into account the multibody hydrodynamic interactions. In such a frame, the governing equation is:

$$m\frac{d\boldsymbol{u}}{dt} = \sum_{j\neq i}\boldsymbol{F_{ij}^C} + \sum_{j\neq i}\boldsymbol{F_{ij}^D} + \sum_{j\neq i}\boldsymbol{F_{ij}^R} \tag{13.33}$$

where $\boldsymbol{F_{ij}^C}$ are the conservative forces acting on particle i due to particle j, $\boldsymbol{F_{ij}^D}$ are the dissipative forces due to the exchange of momentum, and $\boldsymbol{F_{ij}^R}$ are random forces. This method has been used to model a wide variety of multiphase systems at the microscale, such as oil−water interfaces [85], adsorption of surfactants on carbon nanotubes [84], and surfactant structures in solution [13].

The *lattice Boltzmann dynamics* (LBD) models the fluid as if consisting of fictive particles, which perform consecutive propagation and collision processes over a discrete lattice mesh [56]. Usually, the lattice mesh is identified by an acronym DnQm: It is obtained by superposition of a homogeneous Cartesian mesh (D2 when we are in two dimensions) and a finite set of discrete particle velocities (nine for the case of two-dimensional mesh, Q9). As opposed to classical MD methods dealing with positions and velocities of fluid particles, LBD treats the velocity distribution function of particles at each grid point over a discretized domain [74]; time is discretized as well. Fluid particles can collide with each other, as they move according to a set of rules, which are designed in such a manner that the governing continuity and the Navier−Stokes equation are recovered. The collision model typically used in LBD is the Bhatnagar−Gross−Krook model [4].

The LBM method is powerful in dealing with both single and multiphase flow problems, also in complex geometries [44]. In most lattice Boltzmann models, the solid and fluid phases are represented

by a set of lattice sites, and the interface is represented by the edges of lattice sites that separate different phases [52]. Several studies are reported in the literature, which combine LB simulations and pore structure characterization techniques to examine colloid transport in porous media [44]. Due to its particulate nature and local dynamics, LBM has several advantages over other conventional CFD methods, especially in dealing with complex boundaries, incorporating microscopic interactions, and parallelization of the algorithm.

2.3.2 Pore-network models

After the introduction of pore-network modeling by Fatt [23], to calculate flow of fluids in pore network, it has been further applied for transport of solutes and particles in porous media [40,42,82,90,62]. Examples of the recent achievements on the pore-network modeling are to account for relatively weak chemical interactions such as the van der Waals' force, which is often neglected in macroscale models [89], and to combine them with a multiphase flow method [7,26]. Pore-network models are capable of simulating the interactions of nanoparticles, solvent, and soil grains at the pore scale (i.e., applying local hydrogeochemical conditions and local grain surface chemistry information).

Transport through the pore space is modeled applying mass balance equations for each element of the network (i.e., pore bodies and throats). Using pore network modeling, each pore is considered as a fully mixed domain. Therefore, a single concentration is assigned to each pore body or pore throat [70]. For a given pore body (e.g., pore body i in Fig. 13.4), one may write the mass balance equation:

$$V_i \frac{dc_i}{dt} = \sum_{j=1}^{N_{in}} q_{ij} c_{ij} - Q_i c_i \tag{13.34}$$

where c_i is the average concentration of pore i, c_{ij} is the pore throat average concentration, Q_i is the total flux of fluid leaving the pore body, V_i is the volume of pore body, and N_{in} is the number of pore throats flowing into pore body i. As the total water flux entering a pore body is equal to the flux leaving it, we have:

$$Q_i = \sum_{j=1}^{N_{in}} q_{ij} \tag{13.35}$$

Note that, in Eq. (13.34), adsorption of solutes to the pore body walls is neglected. Adsorption of the solutes to the walls of the pore throats is taken into account. The mass transport equation for a given pore throat may be written as:

$$V_{ij} \frac{dc_{ij}}{dt} = |q_{ij}| c_j - |q_{ij}| c_{ij} - V_{ij} k_{att,ij} c_{ij} + V_{ij} k_{\mathrm{det},ij} s_{ij} \tag{13.36}$$

where V_{ij} is the volume of the pore throat, q_{ij} denotes the volumetric flow within the tube, s_{ij} is the average adsorbed concentration, and $k_{att,ij}$ and $k_{det,ij}$ are attachment and detachment rate coefficients of tube ij, respectively. The first term on the right-hand side of Eq. (13.36) accounts for the mass entering from the upstream node j, and the second term is the mass leaving the pore throat into the downstream pore body.

We also need an equation for the adsorbed mass concentration:

$$\frac{ds_{ij}}{st} = k_{att,ij} c_{ij} - k_{\mathrm{det},ij} s_{ij}. \tag{13.37}$$

Combining Eqs. (13.34) through (13.37) results in a linear set of equations to be solved solution concentration as well as concentration of adsorbed mass. After obtaining the solution at each time step, breakthrough curves (BTCs) at a given longitudinal position can be calculated by averaging the concentrations of pores centered at that position. In calculating BTCs, the concentrations of pores can be weighted by their volumetric flow rate, resulting in a flux-averaged concentration.

2.4 Mechanisms of particle–porous medium interactions

Deposition of particles from the bulk of the fluid to the collector surface may be viewed as a two-step process: the transport of the particle from the suspension to the proximity of the surface, and the particle's subsequent adhesion to the surface, which depends on the nature of surface–particle interactions [78]. The transport of colloidal particles from the pore fluid to the vicinity of the collector is typically described by three mechanisms: interception, gravitational sedimentation, and Brownian diffusion [81]. Interception is a steric phenomenon and happens when a particle flowing along a streamline comes close enough to a sand grain; gravitational sedimentation is due to the settling of the particles when their density is higher than the density of water; and Brownian diffusion is caused by the Brownian thermal movement that causes particles to leave a fluid streamline and come into contact with the grain surface. The efficiency of transport by interception and gravity increases with an increase in size of the suspended particles, whereas transport by diffusion increases with a decrease in particle size: This is due to the molecular diffusion being inversely proportional to particle size. In general, under physical conditions typical for water and wastewater filtration, the transport of submicrometric particles is dominated by diffusion, whereas that of larger (non-Brownian) particles is dominated by interception [22]. The second step, properly called *attachment*, is controlled by surface interaction forces that can be described using the Derjaguin–Landau–Verwey–Overbeek (DLVO) theory. Therefore, if the conditions are favorable to deposition (e.g., the net colloidal force is attractive), the transport step controls the rate of deposition. If the conditions are unfavorable (e.g., there is an energy barrier for particles to overcome before being deposited), the deposition step controls the rate of deposition [22].

2.4.1 Forces acting on an uncharged particle

The first step of particle deposition (namely, particle transport from the bulk fluid to the vicinity of the collector is controlled by the forces acting on the particle within the fluid).

The *gravity force* is the algebraic sum of two contributions: the weight of the particle and the buoyancy force (Table 13.1). The simplest formulation for the *drag force* (Table 13.1) proposed holds under general conditions. However, corrections are required when the particle size is comparable with the average free path of fluid particles or when the particle is close to the surface of the collector. In particular, close to the collector surface, the particle velocity differs from the fluid velocity in the same point, and the drag force can be corrected by applying a coefficient called hydrodynamic correction functions [87]. For freely moving particles, the following correction functions were proposed for the force perpendicular and parallel to the collector, respectively:

$$f_1(H) = \frac{19H^2 + 4H}{19H^2 + 26H + 4} \tag{13.38}$$

$$f_4(H) = \frac{1}{1.062 - 0.516\ln(H)} \tag{13.39}$$

where H is the dimensionless distance $H = h/a_p$ (being h the distance between particle and collector, and a_p the particle radius).

The hydrodynamic resistance increases in the presence of macroscopic interfaces due to the viscous resistance to motion exerted on the fluid by the solid. During the movement toward the rigid wall, the liquid is pushed out of the gap between particle and interface, and this phenomenon requires more energy than the drag of the liquid near the rigid wall by the particle (parallel motion). As a consequence, a correction to the components of particle velocity is to be applied. The correction is significantly larger for the velocity component perpendicular to the rigid interface compared with the one applied to the parallel component:

The *Brownian force* (Table 13.1) is usually modeled as a Gaussian white noise process and must be decomposed in normal and tangential components, to take into account the hydrodynamic retardation:

$$F_B^n = R\sqrt{\frac{2\xi_n k_B T}{\Delta t}} \quad \text{with } \xi_n = \frac{6\pi\mu a_p}{f_1(H)}, \tag{13.40}$$

$$F_B^t = R\sqrt{\frac{2\xi_t k_B T}{\Delta t}} \quad \text{with } \xi_t = \frac{6\pi\mu a_p}{f_4(H)}. \tag{13.41}$$

Brownian motion cannot be solved analytically, but rather as a series of uncorrelated random movements. It is worth to mention that for a correct calculation, the time step employed in the trajectory simulation must be much greater than the particle momentum relaxation time, m/ξ, ξ being the friction coefficient and m the particle mass; moreover, the time step must be small enough to consider all forces constant during the time step considered [49].

2.4.2 Interactions among charged bodies: DLVO and extended DLVO theory

The second step of particle deposition, namely adhesion onto the collector, is controlled by surface interactions among collector and particles themselves. The *DLVO theory* defines the interaction potentials between two faced, charged surfaces, which is given by the combined effects of Van der Waals attraction and electrostatic interaction. According to the classical DLVO theory, the interaction potential between two surfaces is the sum of the attractive Van der Waals interaction and the electrostatic interaction (repulsive or attractive):

$$V_{tot} = V_{VdW} + V_{EDL} \tag{13.42}$$

where V indicates the potential energy [J]. Colloids are assumed to be uniform spheres, small relative to the sand grains. In the following, formulas for sphere−plate interactions are reported for calculation

Table 13.1 Mathematical formulation of the forces acting on colloidal particles.

Forces	Mathematical expressions
Gravity force	$\boldsymbol{F_G} = \frac{4}{3}\pi a_p^3(\rho_p - \rho)\boldsymbol{g}$
Drag force	$\boldsymbol{F_D} = 6\pi\mu a_p(\boldsymbol{v} - \boldsymbol{u})$
Brownian force	$\boldsymbol{F_B} = R\sqrt{\frac{2\xi k_b T}{\Delta t}}$

a_p, *particle radius;* ρ_p, *particle density;* ρ, *fluid density;* g, *acceleration of gravity;* v, *fluid velocity;* u, *particle velocity;* R, *random-normal distribution number;* k_B, *Boltzmann constant;* T, *absolute temperature;* ξ, *friction coefficient;* Δt, *simulation time step.*

of particle–collector interactions. Particle–particle interactions are obtained with the sphere–sphere geometry and can be shown to be half the value of sphere–plate interactions (i.e., Derjaguin's approximation) [22].

London-van der Waals forces are generated by spontaneous fluctuating electrical and magnetic polarizations that give rise to an electromagnetic field in the region between the surfaces. The magnitude of these forces depends on material properties of the particles, filter media, and solution. Although a rigorous formulation for interatomic potentials should be based on quantum mechanics, the Van der Waals interaction for a single-species 1:1 electrolyte is usually calculated following the Hamaker approach [22], basing on Gregory's formulation [29].

$$V_{VdW} = -\frac{Aa_p}{6h\left(1+\frac{14h}{\lambda}\right)} \tag{13.43}$$

where A is the Hamaker constant [J] and λ is the characteristic wavelength of the interaction, which accounts for the retardation effect due to the finite time of propagation of the interaction [L]. The value of 100 nm is often used for λ [22]. The formulation is accurate for $h < 0.1a_p$. For larger distances, other formulations are available [22,45]. The Van der Waals force is obtained as $F_{VdW} = -\nabla V_{VdW}$ and is always attractive, acting along the normal to the surface.

The *electrical double layer interaction* is due to the partial overlapping of the diffuse double layers that surround the facing particles or surfaces [50]. Since the charge in the double layer depends on the charge on the particle surface, the interaction for particles of the same material is always repulsive. A number of solutions for the calculation of V_{EDL} are available, each valid over different ranges of distances and under different assumptions. As a general rule, the interaction potential (or the force) depends on the separation distance, the ionic strength, and the charge or potential at each surface. However, analytical formulations depend on the boundary conditions applied at the surfaces. For similarly charged surfaces, the *constant charge approach* (no relaxation of the electric double layer) yields the largest repulsive force or energy barrier, whereas the *constant potential approach* (fully relaxed electric double layer) yields much lower values. An intermediate solution is provided by the *regular surface interaction* [79]. For most natural and synthetic colloids interacting with natural porous media, the assumption of constant potential at the surface (CPA) proposed by Hogg et al. [33] is adopted:

$$V_{EDL} = \varepsilon_0\varepsilon_r\pi a_p\frac{\zeta_p^2+\zeta_c^2}{4}\left[\frac{2\zeta_p\zeta_c}{\zeta_p^2+\zeta_c^2}\ln\left(\frac{1+e^{-\kappa h}}{1-e^{-\kappa h}}\right)+\ln\left(1-e^{-2\kappa h}\right)\right] \tag{13.44}$$

where ζ_p and ζ_c are, respectively, the particle and the collector zeta potential and κ is the Debye–Huckel reciprocal length. The Debye–Huckel reciprocal length κ is calculated as:

$$\kappa = \sqrt{\frac{e^2\sum_i c_{n,i}z_i^2}{\varepsilon k_B T}} \tag{13.45}$$

where e is the electron charge ($-1.602\cdot10^{-19}$ C), $c_{n,i}$ is the bulk number concentration of ions of the i-th type (tied to the ionic strength), and z_i is the valence of the i-th ions. The CPA approach is valid for $\zeta_p \approx \zeta_c < 60$ mV and $\kappa a_c > 5$, and its accuracy decreases for small separation distances.

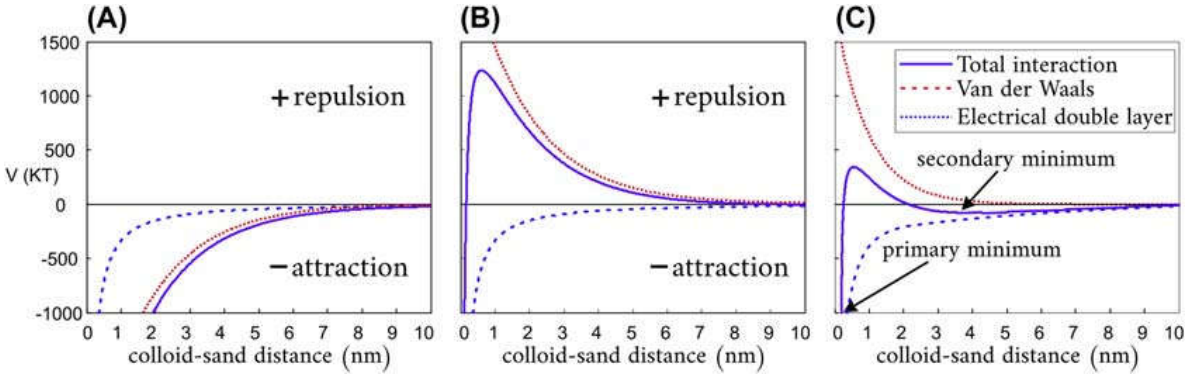

FIGURE 13.5

Example of interaction energy profiles for a sand (plate)—colloid (sphere) system: attractive (A), repulsive (B), and repulsive with attractive secondary minimum (C).

The sum of Van der Waals attraction and electrical double layer repulsion can result in a completely attractive profile, a completely repulsive profile, or in a profile with a primary and a secondary minimum (Fig. 13.5). When particle and sand grains are similarly charged, both Van der Waals and electrical double layer interactions are attractive: no repulsive barrier exists and deposition takes place under favorable conditions. Deposition in the primary minimum leads to irreversible attachment, whereas deposition in the secondary minimum can be reversible. Even moderate changes in solution chemistry may significantly affect the depth of the secondary minimum, thus resulting in particle release. According to the energy barrier approach, the rate of colloid mobilization depends on the height of the barrier in DLVO potential energy that attached colloids must exceed [72]. Electrical interaction between colloidal particles (especially in aqueous systems) is one of the most important influences on particle stability, aggregation, and deposition. In most cases, the only practical means of manipulating the stability of particles and their tendency to deposit on surfaces is by changing the electrical interaction through changes in the solution chemistry.

Beside the two interaction forces considered by the classical DLVO theory, additional interaction forces can be considered, including:

- *Born repulsion*, due to short-range repulsive forces generated by the interpenetration of electron shells, when the surface−surface distance significantly decreases. An estimation for Born repulsion with an accuracy comparable with that of DLVO theory was firstly proposed by Ruckenstein and Prieve [71]. In many real applications, when the presence of adsorbed polymer chains on the surface of colloids is likely to occur, Born repulsion never plays a significant role, as polymers prevent colloids to approach closer than few nanometers or fractions of the nanometer [22].
- *Steric repulsion*, generated in the presence of polymeric chains attached on the solid surface. It is due to a combination of the *osmotic repulsion* and the *elastic repulsion* generated by compression of the brush layer (polymer chains and liquid phase) that surrounds colloidal particles, as they approach each other. A mathematical formulation has been provided by Vincent et al. [86].
- *Magnetic attraction*, which is generated between surfaces with a residual magnetic saturation also in the absence of external magnetic fields. It can be calculated following [19,28,51].

Also for these additional interactions, the hypothesis of linear superposition is usually applied [38].

2.5 From pore- to macroscale: the single collector deposition efficiency

The ultimate aim of pore-scale transport models is to predict the transport and deposition of particles as a function of suspension characteristics, physical and chemical properties of the filter, and flow conditions. Important suspension characteristics include density, size distribution, and surface chemistry of the particles, and temperature, viscosity, and solution chemistry of the suspending medium. The parameters that describe the properties of packed-bed filters are bed depth, grain size, grain shape, grain surface chemistry, and porosity. Another important parameter in packed-bed filtration is the approach (superficial) velocity U, defined as the ratio of the volumetric flow rate to the filter cross-section area [22].

In clean bed filtration [91], the removal of particles is represented by a single or a unit collector removal efficiency, usually denoted as η. The single collector removal efficiency is defined as the ratio of the overall particle deposition rate onto the collector to the convective transport of particles toward the projected area of the collector. For an isolated spherical collector, the single collector removal efficiency is:

$$\eta = \frac{I}{UC_0\left(\pi a_c^2\right)} \tag{13.46}$$

where I is the overall particle deposition rate, U the average approach velocity, and C_0 the average influent particle concentration.

Numerous approaches have been proposed for the calculation of η from microscopic (fundamental) equations. The single collector removal efficiency η can be expressed as a product of the single collector contact efficiently η_0, related to nonchemical processes, and an empirical collision efficiency α, describing the attachment step due to DLVO interactions and other processes not included in η_0:

$$\eta = \alpha\eta_0 \tag{13.47}$$

where η_0 is calculated from microscale equations and α is determined experimentally [22,79].

The deposition of colloids in porous media has been investigated by several researchers to improve existing methods by incorporating the forces such as hydrodynamic and attractive forces into the governing equations [69,81,91]. Both Eulerian and Lagrangian approaches have been proposed to derive an analytical formulation of η (or η_0). The Eulerian approach, since it requires lower computational efforts, was the first approach applied in these studies. On the other hand, the Lagrangian method, based on trajectory analysis, is more computationally demanding and has been widely applied more recently, thanks to the increasing power of computers and sophisticated numerical software. It was first applied to all interception phenomena except Brownian motion, due to the excessive computational requirements [22,79], and only recent studies fully incorporated Brownian motion also in trajectory analysis.

Early studies on the definition of η were carried out using analytical calculations. The first evaluation of particle deposition on a spherical collector due to Brownian diffusion was proposed by Levich [43]. This result was then used by Yao [91], who firstly proposed a complete model to predict particle deposition efficiency due to interception, gravity, and diffusion (respectively, η_I, η_G, and η_D) onto a single spherical collector in an undisturbed vertical flow with no influence of possible surrounding collectors. The formulation of the deposition efficiency was obtained assuming that the three mechanisms are additive, and therefore, η_0 is calculated as

$$\eta_0 = \eta_D + \eta_I + \eta_G \tag{13.48}$$

The assumption of additivity for the deposition efficiency was later on validated by Prieve [68]. The formulations proposed by Yao are

$$\eta_D = 4.04 N_{Pe}^{-2/3} \tag{13.49}$$

$$\eta_I = \frac{3}{2}\left(\frac{a_p}{a_c}\right)^2 \tag{13.50}$$

$$\eta_G = \frac{2}{9}\frac{(\rho_p - \rho) g a_p^2}{\mu U} \tag{13.51}$$

N_{Pe} is the Peclet number, defined as

$$N_{Pe} = \frac{2Ua_c}{D} \tag{13.52}$$

Yao et al. [91] observed discrepancies between their analytical results and their experimental results due to the assumption of infinite fluid domain around the collector and due to the absence of DLVO forces in their formulation. Pfeffer [66] applied the same approach of Yao to a Happel's model, i.e., considering real porosity and flow field of a packed bed, and proposed a modified diffusion term:

$$\eta_D = 4 A_s^{1/3} N_{Pe}^{-2/3} \tag{13.53}$$

where A_S is a porosity-dependent parameter accounting for the hydrodynamic effects of neighboring collectors, defined as [22]

$$A_s = \frac{1(1-\gamma^5)}{2 - 3\gamma + 3\gamma^5 - 2\gamma^6} \tag{13.54}$$

The original interception term proposed by Yao et al. [91] was later corrected by Elimelech [22] by considering also the porosity dependency:

$$\eta_I = \frac{3}{2} A_S \left(\frac{a_p}{a_c}\right)^2 \tag{13.55}$$

As pointed out by Messina et al. [53], the deposition term usually named "Brownian motion," resulting in η_D, is in reality due to the mutual interaction of advection and pure diffusion and was originally derived for Péclet numbers greater than 70. Moreover, the deposition term defined as "interception," η_I, is due to the combination of advection (which alone does not bring to any deposition) and the effect of the particle finite size (steric effect). The gravity deposition term, η_G, is due to the action of pure gravity on the colloidal particles. Fig. 13.6 clarifies how these three deposition mechanisms work.

Rajagopalan and Tien [69] applied a Lagrangian approach (i.e., particle trajectory analysis) in a Happel's model to derive interception and gravity removal efficiencies, whereas Brownian diffusion was treated separately by adding Pfeffer's diffusion term [66] (Eq. 13.53). Electrical double-layer effects were also included, leading to the final formulation of the total collector removal efficiency:

$$\eta = 0.72 A_S N_{LO}^{1/8} N_R^{15/8} + 2.4 \cdot 10^{-3} A_S N_G^{1.2} N_R^{-0.4} + 4 A_S^{1/3} N_{Pe}^{-2/3} \tag{13.56}$$

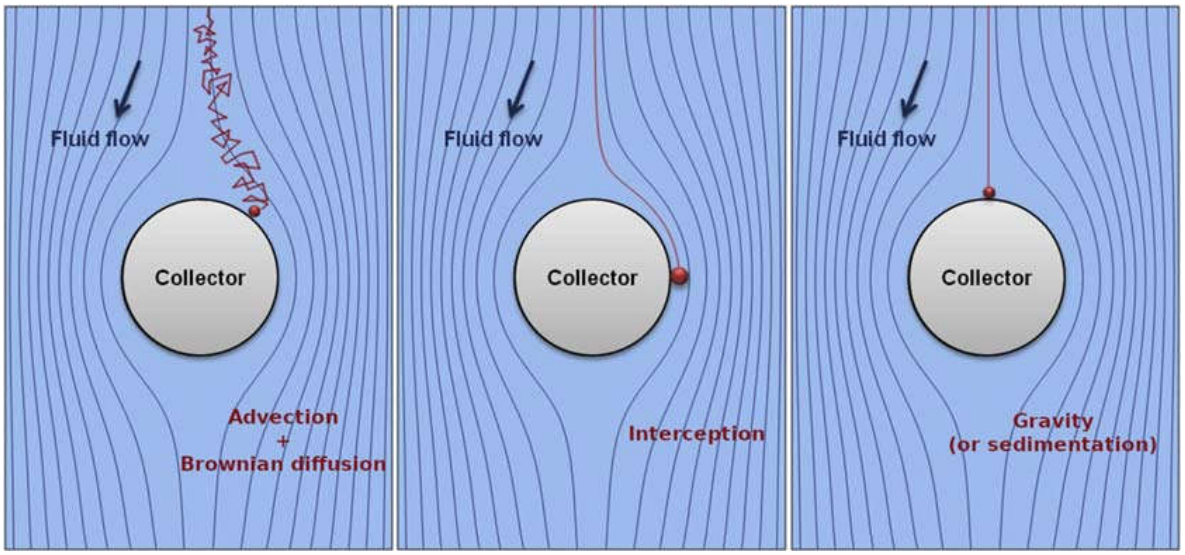

FIGURE 13.6

The three major mechanisms controlling particle deposition onto a collector: gravity, interception (i.e., combination of advection and steric effect), and Brownian motion (i.e., combination of advection and Brownian diffusion).

where N_R is the relative size group, N_{L0} is the London group, and N_G is the gravity group:

$$N_{L0} = \frac{A}{9\pi\mu a_p^2 U} \tag{13.57}$$

$$N_R = \frac{a_p}{a_c} \tag{13.58}$$

$$N_G = \frac{2a_p^2(\rho_c - \rho_f)g}{9\mu U} \tag{13.59}$$

Logan et al. [46] corrected the work of Rajagopalan and Tien and made it consistent with the efficiency definition valid for the Happel's model:

$$\eta_0 = \frac{I}{UC_0(\pi b^2)} \tag{13.60}$$

where b is the radius of the fluid shell in the Happel's model.

Tufenkji and Elimelech [81] developed a closed-form solution for calculating colloid deposition efficiency on a solid grain by combining the approaches of Yao [91] and Rajagopalan and Tien [69]. They accounted for the superposition of the effects of hydrodynamic forces, Van der Waals interactions, and gravity effects and proposed the following correlation equation:

$$\eta_0 = 2.4A_S^{1/3}N_R^{-0.081}N_{Pe}^{-0.715}N_{VdW}^{0.052} + 0.55A_S N_A^{0.125}N_R^{1.675} + 0.22N_R^{-0.24}N_G^{1.11}N_{VdW}^{0.053} \tag{13.61}$$

where N_{VdW} is the Van der Waals number (describing the entity of the Van der Waals interaction energy with respect to the thermal energy of the system) and N_A is the attraction number (characterizing the effects of fluid velocity and Van der Waals interaction on the particle deposition due to interception). These two last ones are defined as

$$N_{VdW} = \frac{A}{k_B T} \tag{13.62}$$

$$N_A = \frac{A}{12\pi U \mu a_p^2} \tag{13.63}$$

The Lagrangian approach has been successfully applied in the past years for a deeper understanding of colloid retention processes. Nelson and Ginn [58] applied a Lagrangian trajectory analysis in Happel's sphere-in-cell geometry with Stokes flow by using the concept of limiting trajectory and considering only deterministic forces, whereas the stochastic Brownian force was added in a second step. Their results are in good agreement with the deterministic trajectory analysis of Rajagopalan and Tien [69] when diffusion is neglected and fit excellently the Levich solution [43] for convective diffusion when external forces and interception are neglected. Conversely, they found that the interaction of Brownian diffusion with sedimentation and interception has a significant effect on η, thus suggesting that the original assumption of additive rule on η does not hold. This conclusion is consistent with the results of Tufenkji and Elimelech [81] for large particles, whereas for submicrometer particles, unexpected discrepancies are found.

The Lagrangian approach was also applied by several authors to elucidate the role of grain-to-grain contacts in particle retention. Cushing and Lawler [18] used a regular packing of spheres to investigate the mutual influence of multiple collectors and showed that contact points play a relevant role in particle retention due to complex hydrodynamic processes, which funnel particles toward them, where particles are stably retained. This model, however, is less sensitive to particles size than experimental data and to the influence of surface chemical properties, likely due to the predominance of hydrodynamic processes at grain-to-grain contacts.

Johnson et al. [36] further elucidated the role of grain-to-grain by means of a three-dimensional particle tracking that predicts colloid retention in porous media in the presence of an energy barrier via two mechanisms, namely, wedging of colloids within grain-to-grain contacts and retention of colloids (without attachment) in flow stagnation zones. Both wedging and retention in flow stagnation zones were sensitive to colloid surface interaction forces (energy barrier height and secondary energy minimum depth). The model provides a mechanistic basis for colloid retention in the presence of an energy barrier via processes that were recently hypothesized to explain experimental observations.

Ma et al. [49] developed a full Lagrangian approach on all physical (drag, gravity, Brownian motion) and chemical (DLVO) forces for particle trajectory analysis in a hemisphere-in-cell model geometry. The flow field was solved numerically via CFD. This choice is justified by the goal of predicting colloid deposition in the presence of energy barriers, which has been shown in previous literature to involve deposition within grain-to-grain contacts for colloid to collector ratios greater than approximately 0.005. A correlation equation for predicting collector efficiencies in the hemispheres-in-cell model in the absence of energy barriers was developed via regression of numerical results to dimensionless parameters [49]:

$$\eta = \gamma^2 \left(2.3 A_S^{1/3} N_R^{-0.08} N_A^{0.052} N_{Pe}^{-0.65} + 0.55 A_S N_A^{0.15} N_R^{1.8} + 0.2 N_R^{-0.10} N_G^{1.1} N_A^{0.053} N_{Pe}^{0.053} \right) \tag{13.64}$$

Song and Elimelech [76] pointed out first some limitations of the existing models for the single collector efficiency, which predict efficiency values greater than one in some particular cases, e.g., for very small or very large particles and/or for very low approach velocities. The authors clarified that this unphysical result is due to the transposition of the boundary conditions from the isolated sphere collector model to the sphere-in-cell model.

Later, Nelson and Ginn [59] proposed the following correlation equation to overcome these limitations:

$$\eta_0 = \gamma^2 \left[2.4 A_S^{1/3} \left(\frac{N_{Pe}}{N_{Pe} + 16} \right)^{0.75} N_{Pe}^{-0.68} N_{Lo}^{0.015} N_{Gi}^{0.8} + A_S N_{Lo}^{1/8} N_R^{15/8} + 0.7 N_G N_R^{-0.05} \left(\frac{N_{Gi}}{N_{Gi} + 0.9} \right) \right] \tag{13.65}$$

where

$$N_{Gi} = \frac{1}{1 + N_G} \tag{13.66}$$

and all the other parameters have been already defined.

They explained these efficiency values above unity as an overestimation of the contribution due to diffusion and sedimentation. Their model was further refined in Nelson et al. [60].

Also Ma et al. [48] proposed a normalized correlation equation:

$$\eta_0 = \gamma^2 \left[\frac{8 + 4(1-\gamma) A_S^{1/3} N_{Pe}^{1/3}}{8 + (1-\gamma) N_{Pe}^{0.97}} N_{Lo}^{0.015} N_{Gi}^{0.8} N_R^{0.028} + A_S N_{Lo}^{15/8} N_R^{1/8} + 0.7 N_R^{-0.05} N_G \left(\frac{N_{Gi}}{N_{Gi} + 0.9} \right) \right] \tag{13.67}$$

Moreover, they explained that the existing correlation equations are valid only for Peclet number between 70 and 10^4.

Messina et al. [53], by performing combined Lagrangian and Eulerian simulations and by modifying the definition of single collector efficiency, proposed a new correlation equation valid for a wide range of parameter (in particular, also for Peclet numbers less than 70). Moreover, the effect of possible interaction between the basic transport and deposition mechanisms (i.e., advection, Brownian deposition, gravity, and the effect of particle finite size) was analyzed, and the proposed model takes all the possible (14) individual and combined deposition mechanisms into account. Two formulations were proposed for the single collector efficiency, namely, a complete formulation, including all the 14 possible interaction mechanisms, and a reduced order model, including only the most important ones:

$$\eta_N = \gamma^2 \frac{\left[1.5062 A_S N_R^{1.9834} + 7.5609 N_{Pe}^{-1}/(2-2\gamma) + N_G + A_S^{0.3662} N_{Pe}^{-0.6338} \left(2.9352 + 2.7480 N_R^{0.3737} \right) + 0.9461 N_G^{0.6550} N_{Pe}^{-0.3450} \right]}{\left[\left(1 + 6.0098 A_S N_R^{1.9834} \right) + \gamma^2 7.5609 N_{Pe}^{-1}/(2-2\gamma) + N_G + A_S^{0.3662} N_{Pe}^{-0.6338} \left(2.9352 + 2.7480 N_R^{0.3737} \right) + 2.7972 N_G^{0.6550} N_{Pe}^{-0.3450} \right]} \tag{13.68}$$

It is finally worth to mention a new trajectory simulation algorithm developed in 2010 by Wei and Wu [88] to describe the efficiency of a single collector (pore) to catch submicrometer particles moving through saturated porous media. A constricted-tube model incorporating the deterministic (interception, hydrodynamic retardation, Van der Waals force, and gravitational sedimentation), stochastic (Brownian diffusion), and thermodynamic (electrostatic and steric repulsion force) mechanisms was established to predict nanoscale zerovalent iron particles transport and deposition by applying a Lagrangian trajectory analytical approach. The simulation results show good agreement with the

results predicted by existing energy barrier—free models, except for particle size lower than 100 nm at low approach velocity. The model successfully described the breakthrough curve of polymer modified nanoscale zerovalent iron in a benchtop soil column as well. The novel simulation scheme can be a useful tool for predicting the behavior of the nanoscale colloidal particles moving through filter beds or saturated soil columns under conditions with repulsion and attraction forces among surfaces.

Models and approaches presented so far all deal with the definition of the removal efficiency of a single collector. However, for practical applications, the efficiency determined for a single grain is to be up-scaled to the entire porous medium. Several approaches have been proposed so fare, whose detailed description is out of the purpose of the present review. As firstly suggested by Payatakes et al. [65], a filter/porous media can be viewed to be an assembly of identical collectors, and the decay of concentration along the filter bed can be obtained as a combination of the removal efficiency of the individual collectors. However, it has been demonstrated [37] that the assumption of constant removal efficiency along the porous bed does not hold under unfavorable deposition conditions.

Even in the case of favorable deposition (i.e., attachment efficiency equal to unity), the calculation of deposition efficiency from a pore-scale perspective is problematic. We noted earlier the issue of neglecting the diffusive flux toward the collector, resulting in increasingly wrong predictions when considering Peclet numbers lower than 70 [53]. In addition to that, and especially noteworthy in the case of these diffusion-dominated regimes, lies the problem of evaluation of the actual concentration driving force: While it is usually taken for granted that $\Delta C = C_\infty$ (where C_∞ is the solute concentration far away from the collector), this is not accurate when the concentration gradient itself is locally varying in the pore-scale control volume [10]. The very common neglection of the difference between the preasymptotic and asymptotic transport regimes also represents another source of error, this time especially in those cases for which it takes a very long time to reach a stationary (i.e., self-similar) solution, thus for higher Peclet numbers [54].

A challenge for the next future will be that of expending effort on further unifying work regarding proper approaches and correlations for a rigorous up-scaling of pore-scale retention processes to the removal efficiency of a filter bed. In this sense, the increased use of detailed pore-scale mechanistic simulations and experimental imaging of particle transport at the pore scale [39,57] can provide a significant step forward in the elucidation of the basic mechanisms controlling particle retention in porous media.

Nomenclature

Symbol	Parameter	Units of measurement
A	Hamaker's constant	J
a_c	Collector radius	m
a_p	Particle radius	m
A_s	Porosity-dependent parameter in η_D	–
b	Radius of fluid envelope in Happel's model	m
c	Fluid-phase particle concentration	mol/m^3

c_i	Average mass concentration in the i-th pore	mol/m^3
c_{ij}	Average mass concentration in the i,j-th pore	mol/m^3
$c_{n,i}$	Bulk number concentration of ions of the i-th type	mol/m^3
C_0	Influent particle concentration	mol/m^3
D	Particle diffusion coefficient tensor	m^2/s
e	Electron charge	C
f_e	External body force exerted on a unit mass of the fluid	N/kg
f_i	Hydrodynamic coefficients of delay ($i = 1,2, \ldots$)	−
F	External force vector	N
F_B	Brownian force	N
F^C	Conservative force	N
F^D	Dissipative force	N
F_D	Drag force	N
F_{EDL}	Electric double layer force	N
F_G	Gravity force	N
F_{ij}	Forces acting on particle i due to particle j	N
F^R	Random force	N
F_{tot}	Total force acting on a particle	N
F_{VdW}	van der waals force	N
g	Acceleration of gravity	m/s^2
h	Particle−collector distance	m
H	Dimensionless particle−collector distance	−
I	Overall particle deposition rate	mol/(m^{2}s)
k	Permeability tensor	m^2
k_B	Boltzman's constant	J/K
k_{att}	Attachment rate	s^{-1}
k_{det}	Detachment rate	s^{-1}
L_0	Characteristic length	m
L	Network length	m
m	Particle mass	kg
n	Porosity	−
N_A	Attraction number	−
N_G	Gravity group	−
N_{Gi}	Modified gravity group	−
N_{L0}	London group	−
N_{Pe}	Pèclet number	−

Continued

N_{Re}	Reynolds number	–
N_R	Relative size group	–
N_{VdW}	van der waals number	–
P	Hydrostatic pressure	N/m^2
$\widetilde{p}$	Dimensionless hydrostatic pressure	N/m^2
P_i	Pressure in the i-th pore	N/m^2
q_{ij}	Volumetric discharge in the i,j-th pore throat	m^3/s
Q	Total discharge through the network	m^3/s
Q_i	Total discharge leaving the i-th pore	m^3/s
r	Radial coordinate	m
r	Position vector	m
R	Random-normal distribution number	–
R_{ij}	Radius of the i,j-th pore throat	m
S	Cross-sectional area of the network perpendicular to the overall flow direction	m^2
T	Absolute temperature	K
u	Particle velocity vector	m/s
U	Flow velocity	m/s
U_0	Characteristic flow velocity	m/s
U_∞	Uniform flow velocity entering Happel's or Kuwabara's cell	m/s
v	Fluid velocity vector	m/s
$\overline{v}$	Average pore water velocity in the network	m/s
$\widetilde{v}$	Dimensionless velocity	–
v_ϕ	Fluid velocity component along ϕ coordinate	m/s
v_r	Fluid velocity components along r coordinate	m/s
v_θ	Fluid velocity components along θ coordinate	m/s
V_i	Volume of the i-th pore	m^3
V_{EDL}	Electrical double-layer potential	V
V_{VdW}	van der waals potential	V
V_{tot}	Total interaction potential	V
z_i	Valence of the i-th ions	–
α	Attachment efficiency	–
γ	Porosity function	–
ε_i	Permittivity of the i-th material	F/m
ε_0	Dielectric constant of the void	F/m
ε_r	Relative dielectric constant of the material	–
ζ_c	Collector zeta potential	V

ζ_p	Particle zeta potential	V
η	Single collector removal efficiency	−
η_0	Single collector contact efficiency	−
η_D	Single collector efficiency due to Brownian diffusion	−
η_G	Single collector efficiency due to gravitational sedimentation	−
η_I	Single collector efficiency due to interception	−
ξ	Friction coefficient (equal to $6\pi\mu a_p$)	Pa·s·m
θ	Tangential coordinate	rad
κ	Debye−Huckel parameter	1/m
λ	Average wavelength of electron oscillation	m
μ	Fluid viscosity	Pa·s
ρ	Fluid density	kg/m^3
ρ_f	Fluid density	kg/m^3
ρ_p	Particle density	kg/m^3

Acknowledgments

This work was cofunded by the EU research project NanoRem (FP7, GA n. 309517).

References

[1] R.J. Adler, J.E. Taylor, Random fields and geometry, in: Springer monographs in mathmatics, 115, Springer, New York, 2007.
[2] B.J. Alder, D.M. Gass, T.E. Wainwright, Studies in molecular dynamics. VIII. The transport coefficients for a hard-sphere fluid, J. Chem. Phys. 53 (10) (1970) 3813−3826.
[3] B.J. Alder, T.E. Wainwright, Studies in molecular dynamics. I. General method, J. Chem. Phys. 31 (2) (1959) 459−466.
[4] P.L. Bhatnagar, E.P. Gross, M. Krook, A model for collision processes in gases. I. Small amplitude processes in charged and neutral one-component systems, Phys. Rev. 94 (3) (1954) 511−525.
[5] M. Blunt, P. King, Macroscopic parameters from simulations of pore scale flow, Phys. Rev. 42 (8) (1990) 4780.
[6] M.J. Blunt, Flow in porous media — pore-network models and multiphase flow, Curr. Opin. Colloid Interface Sci. 6 (3) (2001) 197−207, https://doi.org/10.1016/S1359-0294(01)00084-X.
[7] M.J. Blunt, M.D. Jackson, M. Piri, P.H. Valvatne, Detailed physics, predictive capabilities and macroscopic consequences for pore-network models of multiphase flow, Adv. Water Resour. 25 (8) (2002) 1069−1089.
[8] G. Boccardo, D.L. Marchisio, R. Sethi, Microscale simulation of particle deposition in porous media, J. Colloid Interface Sci. 417 (0) (2014) 227−237, https://doi.org/10.1016/j.jcis.2013.11.007.

[9] G. Boccardo, F. Augier, Y. Haroun, D. Ferre, D.L. Marchisio, Validation of a novel open-source work-flow for the simulation of packed-bed reactors, Chem. Eng. J. 279 (2015) 809–820.
[10] G. Boccardo, E. Crevacore, R. Sethi, M. Icardi, A robust upscaling of the effective particle deposition rate in porous media, J. Contam. Hydrol. 212 (2018) 3–13.
[11] G. Boccardo, I.M. Sokolov, A. Paster, An improved scheme for a Robin boundary condition in discrete-time random walk algorithms, J. Comput. Phys. 374 (2018) 1152–1165.
[12] G. Boccardo, R. Sethi, D.L. Marchisio, Fine and ultrafine particle deposition in packed-bed catalytic reactors, Chem. Eng. Sci. 198 (2019a) 290–304.
[13] G. Boccardo, A. Buffo, D. Marchisio, Simulation of mixing in structured fluids with Dissipative Particle Dynamics and validation with experimental data, Chem. Eng. Technol. (2019), https://doi.org/10.1002/ceat.201800731.
[14] H. Brinkman, A calculation of the viscosity and the sedimentation constant for solutions of large chain molecules taking into account the hampered flow of the solvent through these molecules, Physica 13 (8) (1947) 447–448.
[15] S. Bryant, M. Blunt, Prediction of relative permeability in simple porous media, Phys. Rev. 46 (4) (1992) 2004–2011.
[16] E. Crevacore, G. Boccardo, D. Marchisio, R. Sethi, Microscale colloidal transport simulations for groundwater remediation, Chem. Eng. Trans. 47 (2016) 271–276.
[17] E. Crevacore, T. Tosco, R. Sethi, G. Boccardo, D.L. Marchisio, Recirculation zones induce non-Fickian transport in three-dimensional periodic porous media, Phys. Rev. 94 (5) (2016) 053118.
[18] R.S. Cushing, D.F. Lawler, Depth Filtration: fundamental investigation through three-dimensional trajectory analysis, Environ. Sci. Technol. 32 (23) (1998) 3793–3801, https://doi.org/10.1021/es9707567.
[19] J. de Vicente, A.V. Delgado, R.C. Plaza, J.D.G. Durán, F. González-Caballero, Stability of cobalt ferrite colloidal particles. Effect of pH and applied magnetic fields, Langmuir 16 (21) (2000) 7954–7961.
[20] D. Ding, D.A. Benson, A. Paster, D. Bolster, Modeling bimolecular reactions and transport in porous media via particle tracking, Adv. Water Resour. 53 (2013) 56–65.
[21] M. Elimelech, Particle deposition on ideal collectors from dilute flowing suspensions: mathematical formulation, numerical solution, and simulations, Sep. Technol. 4 (4) (1994) 186–212, https://doi.org/10.1016/0956-9618(94)80024-3.
[22] M. Elimelech, X. Jia, J. Gregory, R. Williams, Particle Deposition and Aggregation : Measurement, Modelling, and Simulation. Colloid and Surface Engineering Series, Butterworth-Heinemann, Oxford England ; Boston, 1995.
[23] I. Fatt, The network model of porous media, SPE 574-G 207 (1956) 144–181.
[24] D.H. Fenwick, M.J. Blunt, Three-dimensional modeling of three phase imbibition and drainage, Adv. Water Resour. 21 (2) (1998) 121–143.
[25] J.H.P.M. Ferziger, Computational Methods for Fluid Dynamics, Springer, 1999.
[26] M. Flury, H. Qiu, Modeling colloid-facilitated contaminant transport in the vadose zone, Vadose Zone J. 7 (2) (2008) 682–697.
[27] D. Frenkel, B. Smit, Understanding Molecular Simulation: From Algorithms to Applications, Vol. 1, Academic press, 2001.
[28] J. Garcia-Otero, M. Porto, J. Rivas, A. Bunde, Influence of dipolar interaction on magnetic properties of ultrafine ferromagnetic particles, Phys. Rev. Lett. 84 (1) (2000) 167–170.
[29] J. Gregory, Approximate expressions for retarded vanderwaals interaction, J. Colloid Interface Sci. 83 (1) (1981) 138–145.
[30] J. Happel, Viscous flow in multiparticle systems: slow motion of fluids relative to beds of spherical particles, AIChE J. 4 (2) (1958) 197–201, https://doi.org/10.1002/aic.690040214.

[31] J. Happel, H. Brenner, Low Reynolds number hydrodynamics with special applications to particulate media, 1st pbk, in: Mechanics of Fluids and Transport Processes V. 1, M. Nijhoff, The Hague, 1983.
[32] W.K. Hastings, Monte Carlo sampling methods using Markov chains and their applications, Biometrika 57 (1) (1970) 97−109, https://doi.org/10.1093/biomet/57.1.97.
[33] R. Hogg, T.W. Healy, D.W. Fuerstenau, Mutual coagulation of colloidal dispersions, Trans. Faraday Soc. 62 (1966) 1638.
[35] M. Icardi, G. Boccardo, D.L. Marchisio, T. Tosco, R. Sethi, Pore-scale simulation of fluid flow and solute dispersion in three-dimensional porous media, Phys. Rev. 90 (1) (2014) 013032.
[36] W. Johnson, X. Li, G. Yal, Colloid retention in porous media: mechanistic confirmation of wedging and retention in zones of flow stagnation, Environ. Sci. Technol. 41 (4) (2007) 1279−1287.
[37] W.P. Johnson, M. Hilpert, Upscaling colloid transport and retention under unfavorable conditions: linking mass transfer to pore and grain topology, Water Resour. Res. 49 (9) (2013) 5328−5341, https://doi.org/10.1002/Wrcr.20433.
[38] Y. Kamiyama, J. Israelachvili, Effect of ph and salt on the adsorption and interactions of an amphoteric polyelectrolyte, Macromolecules 25 (19) (1992) 5081−5088.
[39] A.A. Keller, M. Auset, A review of visualization techniques of biocolloid transport processes at the pore scale under saturated and unsaturated conditions, Adv. Water Resour. 30 (6−7) (2007) 1392−1407, https://doi.org/10.1016/j.advwatres.2006.05.013.
[40] J. Koplik, T. Lasseter, Two-phase flow in random network models of porous media, Soc. Petrol. Eng. J. 25 (1) (1985) 89−100.
[41] S. Kuwabara, The forces experienced by randomly distributed parallel circular cylinders or spheres in a viscous flow at small Reynolds numbers, J. Phys. Soc. Jpn. 14 (4) (1959) 527−532.
[42] R. Larson, L. Scriven, H. Davis, Percolation theory of two phase flow in porous media, Chem. Eng. Sci. 36 (1) (1981) 57−73.
[43] V.G. Levich, Physicochemical Hydrodynamics. Prentice-Hall International Series in the Physical and Chemical Engineering Sciences, Prentice-Hall, Englewood Cliffs, N.J., 1962.
[44] Z. Li, D. Zhang, X. Li, Tracking colloid transport in porous media using discrete flow fields and sensitivity of simulated colloid deposition to space discretization, Environ. Sci. Technol. 44 (4) (2010) 1274−1280, https://doi.org/10.1021/es9027716.
[45] E.M. Lifshitz, Theory of molecular attractive forces, Sov. Phys. - JETP 2 (1956) 73−83.
[46] B.E. Logan, D.G. Jewett, R.G. Arnold, E.J. Bouwer, C.R. O'Melia, Clarification of clean-bed filtration models, J. Environ. Eng. 121 (12) (1995) 869−873.
[47] M.I. Lowry, C.T. Miller, Pore-scale modeling of nonwetting-phase residual in porous media, Water Resour. Res. 31 (3) (1995) 455−473.
[48] H.L. Ma, M. Hradisky, W.P. Johnson, Extending applicability of correlation equations to predict colloidal retention in porous media at low fluid velocity, Environ. Sci. Technol. 47 (5) (2013) 2272−2278.
[49] H.L. Ma, J. Pedel, P. Fife, W.P. Johnson, Hemispheres-in-Cell geometry to predict colloid deposition in porous media, Environ. Sci. Technol. 43 (22) (2009) 8573−8579, https://doi.org/10.1021/Es901242b.
[50] J.H. Masliyah, S. Bhattacharjee, Electrokinetic and Colloid Transport Phenomena, Wiley-Interscience, Hoboken, N.J, 2006.
[51] E. Matijevic, Surface and Colloid Science, Wiley, New York, 1971.
[52] P. Meakin, A.M. Tartakovsky, Modeling and simulation of pore-scale multiphase fluid flow and reactive transport in fractured and porous media, Rev. Geophys. 47 (3) (2009) RG3002, https://doi.org/10.1029/2008rg000263.
[53] F. Messina, D.L. Marchisio, R. Sethi, An extended and total flux normalized correlation equation for predicting single-collector efficiency, J. Colloid Interface Sci. 446 (2015) 185−193.

[54] F. Messina, T. Tosco, R. Sethi, On the failure of upscaling the single-collector efficiency to the transport of colloids in an array of collectors, Water Resour. Res. 52 (7) (2016) 5492−5505.
[55] N. Metropolis, A.W. Rosenbluth, M.N. Rosenbluth, A.H. Teller, E. Teller, Equation of state calculations by fast computing machines, J. Chem. Phys. 21 (6) (1953) 1087−1092, https://doi.org/10.1063/1.1699114.
[56] S.K. Mitra, S. Chakraborty, Microfluidics and Nanofluidics Handbook: Chemistry, Physics, and Life Science Principles, CRC Press, 2012.
[57] I.L. Molnar, W.P. Johnson, J.I. Gerhard, C.S. Willson, D.M. O'Carroll, Predicting colloid transport through saturated porous media: a critical review, Water Resour. Res. 51 (9) (2015) 6804−6845, https://doi.org/10.1002/2015wr017318.
[58] K.E. Nelson, T.R. Ginn, Colloid filtration theory and the Happel sphere-in-cell model revisited with direct numerical simulation of colloids, Langmuir 21 (6) (2005) 2173−2184, https://doi.org/10.1021/la048404i.
[59] K.E. Nelson, T.R. Ginn, New collector efficiency equation for colloid filtration in both natural and engineered flow conditions, Water Resour. Res. 47 (2011). Artn W05543Doi 10.1029/2010wr009587.
[60] K.E. Nelson, T.R. Ginn, T. Kemai, Comment on "extending applicability of correlation equations to predict colloidal retention in porous media at low fluid velocity", Environ. Sci. Technol. 47 (14) (2013) 8078−8079, https://doi.org/10.1021/Es401944q.
[61] P.-E. ØRen, S. Bakke, Process based reconstruction of sandstones and prediction of transport properties, Transp. Porous Media 46 (2−3) (2002) 311−343, https://doi.org/10.1023/a:1015031122338.
[62] P.-E. Øren, S. Bakke, O.J. Arntzen, Extending predictive capabilities to network models, SPE J. 3 (4) (1998) 324−336.
[63] B. Partopour, A.G. Dixon, An integrated workflow for resolved-particle packed bed models with complex particle shapes, Powder Technol. 322 (2017) 258−272.
[64] A. Paster, D. Bolster, D.A. Benson, Particle tracking and the diffusion-reaction equation, Water Resour. Res. 49 (1) (2013) 1−6.
[65] A. Payatake, C. Tien, R.M. Turian, New model for granular porous media - model formulation, AIChE J. 19 (1) (1973) 58−67, https://doi.org/10.1002/aic.690190110.
[66] R. Pfeffer, Heat and mass transport in multiparticle systems, Ind. Eng. Chem. Fundam. 3 (4) (1964) 380−383, https://doi.org/10.1021/i160012a018.
[67] M. Pilotti, Generation of realistic porous media by grains sedimentation, Trans. Porous Media 33 (3) (1998) 257−278, https://doi.org/10.1023/a:1006598029153.
[68] D.C. Prieve, E. Ruckenstein, Effect of London forces upon the rate of deposition of Brownian particles, AIChE J. 20 (6) (1974) 1178−1187, https://doi.org/10.1002/aic.690200618.
[69] R. Rajagopalan, C. Tien, Trajectory analysis of deep-bed filtration with the sphere-in-cell porous media model, AIChE J. 22 (3) (1976) 523−533, https://doi.org/10.1002/aic.690220316.
[70] A. Raoof, H. Nick, S. Hassanizadeh, C. Spiers, PoreFlow: a complex pore-network model for simulation of reactive transport in variably saturated porous media, Comput. Geosci. 61 (2013) 160−174.
[71] E. Ruckenstein, D.C. Prieve, Adsorption and desorption of particles and their chromatographic-separation, AIChE J. 22 (2) (1976) 276−283.
[72] J.N. Ryan, M. Elimelech, Colloid mobilization and transport in groundwater, Colloid. Surface. Physicochem. Eng. Aspect. 107 (1996) 1−56.
[73] J.E. Saiers, J.N. Ryan, Colloid deposition on non-ideal porous media: the influences of collector shape and roughness on the single-collector efficiency, Geophys. Res. Lett. 32 (21) (2005) L21406, https://doi.org/10.1029/2005gl024343.
[74] A. Satoh, Introduction to Practice of Molecular Simulation, 2011.
[75] A. Singhal, S. Cloete, S. Radl, R. Quinta-Ferreira, S. Amini, Heat transfer to a gas from densely packed beds of monodisperse spherical particles, Chem. eng. j. 314 (2017) 27−37.

[76] L.F. Song, M. Elimelech, Deposition of Brownian particles in porous-media - modified boundary-conditions for the sphere-in-cell model, J. Colloid Interface Sci. 153 (1) (1992) 294–297, https://doi.org/10.1016/0021-9797(92)90321-C.
[77] W.C. Swope, H.C. Andersen, P.H. Berens, K.R. Wilson, A computer simulation method for the calculation of equilibrium constants for the formation of physical clusters of molecules: application to small water clusters, J. Chem. Phys. 76 (1) (1982) 637–649, https://doi.org/10.1063/1.442716.
[78] C. Tien, Granular Filtration of Aerosols and Hydrosols. Butterworths Series in Chemical Engineering, Butterworths, Boston, 1989.
[79] J.E. Tobiason, C.R. O'Melia, Physicochemical aspects of particle removal in depth filtration, J. Am. Water Works Assoc. 80 (12) (1988) 54–64.
[80] T. Tosco, D.L. Marchisio, F. Lince, R. Sethi, Extension of the Darcy-forchheimer law for shear-thinning fluids and validation via pore-scale flow simulations, Trans. Porous Media 96 (1) (2013) 1–20.
[81] N. Tufenkji, M. Elimelech, Correlation equation for predicting single-collector efficiency in physico-chemical filtration in saturated porous media, Environ. Sci. technol. 38 (2) (2004) 529–536.
[82] L. Vasilyev, A. Raoof, J.M. Nordbotten, Effect of mean network coordination number on dispersivity characteristics, Transp. Porous Media 95 (2) (2012) 447–463, https://doi.org/10.1007/s11242-012-0054-5.
[83] L. Verlet, Computer "experiments" on classical fluids. I. Thermodynamical properties of Lennard-Jones molecules, Phys. Rev. 159 (1) (1967) 98–103.
[84] M.D. Vo, B. Shiau, J.H. Harwell, D.V. Papavassiliou, Adsorption of anionic and non-ionic surfactants on carbon nanotubes in water with dissipative particle dynamics simulation, J. Chem. Phys. 144 (20) (2016) 204701.
[85] T.V. Vu, D.V. Papavassiliou, Oil-water interfaces with surfactants: a systematic approach to determine coarse-grained model parameters, J. Chem. Phys. 148 (20) (2018) 204704.
[86] B. Vincent, J. Edwards, S. Emmett, A. Jones, Depletion flocculation in dispersions of sterically-stabilized particles (soft spheres), Colloid. Surface. 18 (2–4) (1986) 261–281.
[87] P. Warszyński, Coupling of hydrodynamic and electric interactions in adsorption of colloidal particles, Adv. Colloid Interface Sci. 84 (1–3) (2000) 47–142, https://doi.org/10.1016/S0001-8686(99)00015-9.
[88] Y.-T. Wei, S.-c. Wu, Development of a trajectory model for predicting attachment of submicrometer particles in porous media: stabilized NZVI as a case study, Environ. Sci. Technol. 44 (23) (2010) 8996–9002, https://doi.org/10.1021/es102191b.
[89] J. Wells, D. Brinkman, K. Stirling, Groundwater contamination from refinery operations: final report.[Fate and transport of hydrocarbons in groundwater], in: National Inst. For Petroleum and Energy Research, Bartlesville, OK, USA, 1988.
[90] D.P. Yale, A. Nur, Network modeling of flow storage and deformation in porous rocks, in: 1985 SEG Annual Meeting, Society of Exploration Geophysicists, 1985.
[91] K.-M. Yao, M.T. Habibian, C.R. O'Melia, Water and waste water filtration. Concepts and applications, Environ. Sci. Technol. 5 (11) (1971) 1105–1112, https://doi.org/10.1021/es60058a005.
[92] A. Zeinijahromi, A. Vaz, P. Bedrikovetsky, Well impairment by fines migration in gas fields, J. Petrol. Sci. Eng. 88 (2012) 125–135.